$\nu i_{13/2}$ structures in ^{155}Sm and ^{159}Gd: Supporting evidence of a $Z = 60$ deformed subshell gap

D. J. Hartley [1], F. G. Kondev,[2] M. P. Carpenter,[2] R. V. F. Janssens,[3,4] M. A. Riley,[5] K. Villafana,[5,*] K. Auranen,[2]
A. D. Ayangeakaa,[3,4] J. S. Baron,[5] A. J. Boston,[6] J. A. Clark,[2] J. P. Greene,[2] J. Heery,[6] C. R. Hoffman,[2] T. Lauritsen,[2] J. Li,[2,†]
D. Little,[3] E. S. Paul,[6] G. Savard,[2] D. Seweryniak,[2] J. Simpson,[7] S. Stolze,[2] G. L. Wilson,[8] J. Wu,[2] and S. Zhu[2,‡]

[1]*Department of Physics, U.S. Naval Academy, Annapolis, Maryland 21402, USA*
[2]*Physics Division, Argonne National Laboratory, Lemont, Illinois 60439, USA*
[3]*Department of Physics and Astronomy, University of North Carolina, Chapel Hill, North Carolina 27599, USA*
[4]*Triangle Universities Nuclear Laboratory, Duke University, Durham, North Carolina 27708, USA*
[5]*Department of Physics, Florida State University, Tallahassee, Florida 32306, USA*
[6]*Department of Physics, Oliver Lodge Laboratory, University of Liverpool, Liverpool L69 7ZE, United Kingdom*
[7]*Nuclear Physics Group, STFC Daresbury Laboratory, Daresbury, Warrington WA4 4AD, United Kingdom*
[8]*Department of Physics and Astronomy, Louisiana State University, Baton Rouge, Louisiana 70803, USA*

Maximal ground-state deformation should occur when both proton and neutron Fermi surfaces are located at midshell. However, subshell gaps that stabilize large deformation can exist at proton or neutron values other than midshell. One such gap may occur at $Z = 60$ in the rare-earth region, as the energy of the first 2^+ states in even-even nuclei are often lowest in an isotonic chain for neodymium ($Z = 60$) rather than the midshell isotopes of dysprosium ($Z = 66$). Further evidence of this deformed gap has now been observed by investigating the signature splitting systematics of the $\nu i_{13/2}$ bands found in the odd-N, rare-earth nuclei. These were aided by the present observation of the $\nu i_{13/2}$ band in ^{159}Gd and the confirmation of the same structure in ^{155}Sm via the transfer of a neutron from a ^{160}Gd beam to a ^{154}Sm target.

I. INTRODUCTION

It is well known that the location of the proton and neutron Fermi surfaces plays a large role in the ground-state deformation of nuclei. In particular, deformation increases as the proton and/or neutron numbers move away from the spherical magic numbers. As a result, it has long been assumed that the maximum ground-state deformation likely occurs at the midpoint (or midshell) between the magic numbers. Therefore, ^{170}Dy would have the largest ground-state deformation in the rare-earth region as its proton number, $Z = 66$, and neutron number, $N = 104$, correspond to midshell between the $Z = 50$ and 82, and the $N = 82$ and 126 spherical shell gaps, respectively.

The evolution of deformation along an isotopic or isotonic chain can be observed in the excitation energies of levels near the ground state. The most commonly known effect is the lowering of the first 2^+ state in even-even nuclei as they become progressively deformed. Indeed, one can observe this trend in rare-earth nuclei through systematic plots such as

Fig. 4 in Ref. [1] or Fig. 5 in Ref. [2], where the energy of the first 2^+ state is generally lower as N increases towards 104. However, a local minimum is found in these figures for energies in the $N = 98$ isotones of samarium, gadolinium, and dysprosium nuclei, which suggests the presence of a subshell gap associated with large deformation [2].

In order to observe how deformation changes with Z, the energy of the first excited 2^+ states of the even-even, rare-earth nuclei have been plotted versus proton number in Fig. 1. An expected decrease of $E(2^+)$ is observed as the proton numbers are reduced from $Z = 70$ (Yb) to $Z = 66$ (Dy). However, in each of the isotonic chains, the energy of the first 2^+ state continues to decrease down to $Z = 60$ (Nd) and can be observed to increase beyond this Z value in the $N = 92$, 94, and 96 chains. Similar to the identification of a localized subshell gap at $N = 98$ noted above, Fig. 1 indicates that a deformed shell gap at $Z = 60$ likely occurs, as already pointed out in Refs. [3–6].

While the systematics of the 2^+ energies along these isotonic chains certainly provides compelling evidence that dysprosium will not have the maximum deformation, it is useful to explore other experimental observables that may provide additional insight about the proton deformed subshell gap in this region. Urban *et al.* [7] recently investigated the systematics of the $E(4^+)/E(2^+)$ energy ratios of the rare-earth, even-even nuclei which also indicate that the $Z = 66$ dysprosium nuclei do not appear to be maximally deformed for $N = 90$, 92, 94, 96, and 98. In the present work, additional
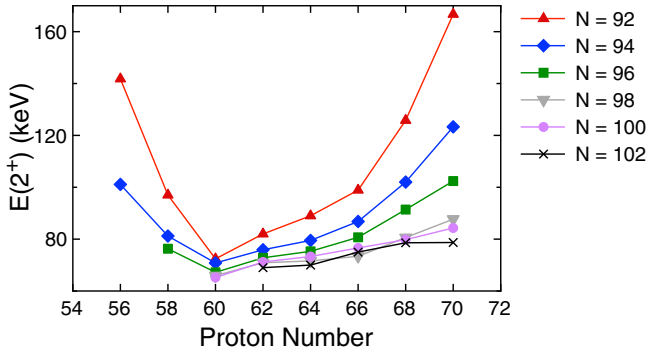
FIG. 1. Energy of the lowest 2^+ states of the even-even nuclei in the rare-earth region plotted versus proton number.
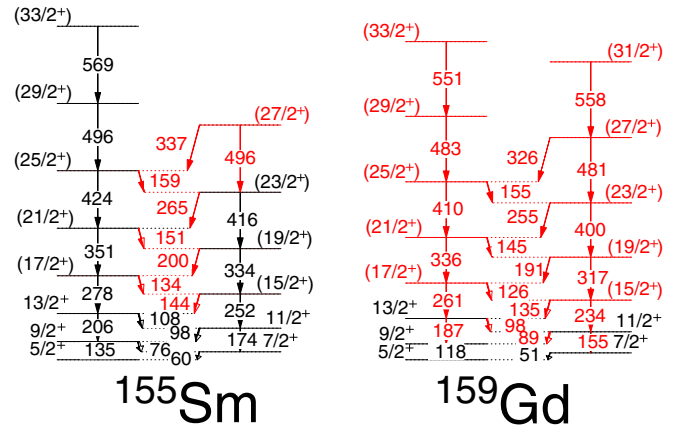

FIG. 2. Level schemes for the $\nu i_{13/2}$ structures in ^{155}Sm and ^{159}Gd. New transitions and levels are shown in red. Note that the 60- and 569-keV transitions in ^{155}Sm as well as the 51- and 118-keV transitions in ^{159}Gd could not be confirmed in these data, but have been observed in other studies.

experimental evidence of the $Z = 60$ gap is presented by examining the signature splitting systematics observed in the $\nu i_{13/2}$ bands of odd-N, rare-earth isotopes.

The $\nu i_{13/2}$ bands in ^{155}Sm and ^{159}Gd were observed in an experiment where the multinucleon transfer process between a ^{160}Gd beam and a ^{154}Sm target populated neutron-rich, rare-earth nuclei. Previously observed transitions in ^{155}Sm [8] were confirmed, while the $\nu i_{13/2}$ structure in ^{159}Gd was extended from spin 13/2 to 33/2.

II. EXPERIMENT

A ^{160}Gd beam, accelerated to 1000 MeV, bombarded a thick ($\sim$240 mg/cm^2) ^{154}Sm target such that all of the reaction products were stopped in the target material. The beam was provided by the ATLAS facility of Argonne National Laboratory, and the resulting γ-ray transitions were detected by 73 detectors in the Gammasphere spectrometer [9]. Although a beam-pulsing condition was used, only the in-beam portion of the data was utilized for the present results. A single-neutron exchange process produced the data for ^{155}Sm and ^{159}Gd where a neutron from the beam nucleus was transferred to the target one. In this process, the transitions for both nuclei are emitted at the same time, and are therefore mutually coincident. The data were sorted into a coincidence cube and analyzed with the RADWARE software package [10]. Unfortunately, there was insufficient data to perform an angular correlation analysis in order to determine the electromagnetic nature of the newly observed transitions. Therefore, tentative spin/parity assignments are proposed based on the assumption that typical rotational behavior occurs above the states that were previously assigned these quantum numbers.

III. LEVEL SCHEMES

The $\nu i_{13/2}$ structure in ^{155}Sm is based on the 2.8(5) μs isomer at 16.5 keV [11]. Asztalos *et al.* [8] were able to extend this sequence to 33/2 in a deep-inelastic experiment; however, no $\Delta I = 1$ transitions between the signature partners were presented in their work. Other studies reported some of the lowest lying $\Delta I = 1$ transitions [12].

The $\nu i_{13/2}$ band-head state in ^{159}Gd is also isomeric [26.2(8) ns], and lies at an excitation energy of 67.8 keV [13].

However, far less was known about the rotational states in this nucleus as it has only been observed up to a spin of 13/2 via transfer reaction experiments [13].

Figure 2 displays the band structures based on the $i_{13/2}$ quasineutron in ^{155}Sm and ^{159}Gd resulting from the current analysis. New transitions and levels are displayed in red. These were the only sequences observed in each of these nuclides. They are both likely to be the yrast sequences and, therefore, they are the most strongly populated by the reaction. Many of the previous transitions in ^{155}Sm which were indicated as tentative by Asztalos *et al.* [8] were confirmed by this experiment (up to 29/2), and the $\alpha = -1/2$ signature was extended to 27/2. In addition, many of the $\Delta I = 1$ connecting transitions between the signature partners were identified. Figure 3(a) displays a summed coincidence spectrum that provides evidence of this structure. As stated above, ^{159}Gd was produced in the same one-neutron exchange reaction as ^{155}Sm; therefore, transitions from the latter nucleus should be observed when coincidence gates are placed on ^{155}Sm γ rays. Indeed, the peaks labeled as "Gd" in Fig. 3(a) are associated with the ^{159}Gd structure.

The only known transitions in the ^{159}Gd sequence connect the 9/2 and 7/2 states to the 5/2 band-head, but were tentatively assigned [13]. However, transfer reactions identified higher spin states, and the current data confirmed their placement through the observation of the corresponding γ-ray transitions from the 11/2 and 13/2 levels. The spectrum in Fig. 3(b) displays how the $\nu i_{13/2}$ ^{159}Gd sequence was extended to a spin of $I = 33/2$. These γ rays are also in coincidence with transitions from the ^{155}Sm structure, which are labeled with "Sm", and, therefore, further provide evidence that this band is properly assigned to ^{159}Gd.

The spins and positive-parity assignments for the lower spin states of both bands have been previously established by various experiments [12,13]. As stated above, all of the spin assignments for the newly observed levels were made based on the assumption that normal rotational behavior persists
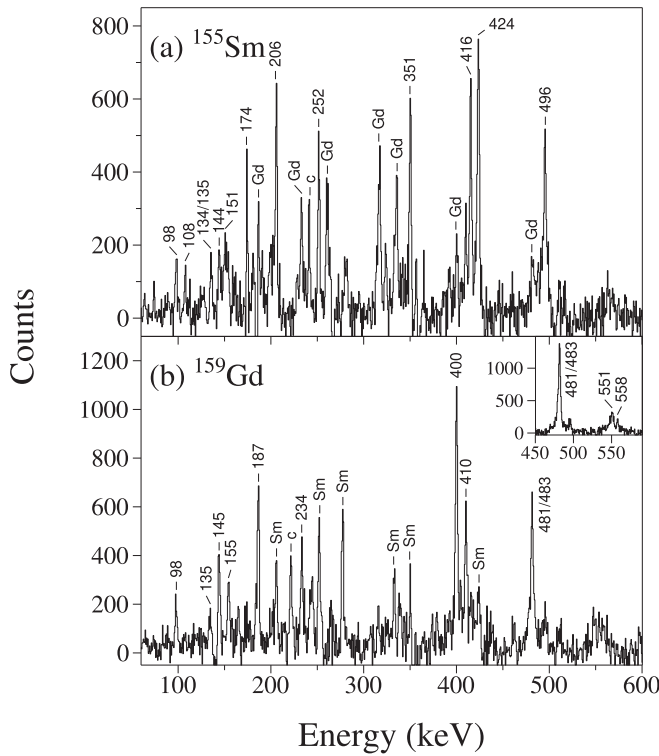
FIG. 3. Coincidence spectra for the $\nu i_{13/2}$ sequences in (a) ^{155}Sm and (b) ^{159}Gd. (a) is a result of spectra from a coincidence cube where the transitions shown result from the summing of the 134/252, 144/334, and 151/334 gates. (b) was constructed in a similar way as (a), where the 191/261, 126/336, and 135/317 gates were summed together. The spectrum in the inset resulted from summing the 234/400 and 261/410 coincidence gates together in order to display the highest observed states. Note that in (a) transitions from ^{159}Gd are denoted with "Gd", and that in (b) transitions from ^{155}Sm are denoted with "Sm".

to the highest observed states. The proposed spin/parity and energy of levels in ^{155}Sm and ^{159}Gd are given in Table I, along with the associated γ-ray transition energies and branching ratios. The positive-parity assignment naturally leads to a $\nu i_{13/2}$ configuration assignment, as this is typically the energetically lowest, positive-parity orbital in this region. However, further evidence for this assignment can be found by observing its distinctive alignment properties, as discussed below.

IV. DISCUSSION

The rotational alignments of the $\nu i_{13/2}$ bands in the $N = 91$, 93, 95, and 97 isotones of Sm, Gd, and Dy [8,14–18] are presented in Fig. 4. In each case, the alignment of the ground-state band from the even-even core nucleus (with $N-1$ neutrons) is also plotted (as empty squares) to demonstrate that appropriate Harris parameters [19] were chosen for the odd-N nuclei as the initial alignment values of the even-even nuclei are approximately 0 $\hbar$. The energetically favored $\alpha = +1/2$ signatures of the $i_{13/2}$ bands are presented as solid

TABLE I. Level and γ-ray energies, along with branching ratios (λ) in ^{155}Sm and ^{159}Gd from the present work. Uncertainties in γ-ray energies are 0.2 keV for transitions reported to the tenths of keV. For γ rays reported to a keV, an uncertainty of 1 keV is assigned.

$I^{\pi\,a}$	E_{level} (keV)	E_γ (keV)	$\lambda^{\,b}$
		^{155}Sm	
$5/2^+$	16.5		
$7/2^+$	76.3		
$9/2^+$	151.9	135.4	0.34(3)
		75.6	
$11/2^+$	250.3	174.0	
		98.4	
$13/2^+$	358.2	206.3	1.22(17)
		108.0	
$(15/2^+)$	502.5	252.2	1.57(10)
		144.3	
$(17/2^+)$	636.4	278.2	3.3(4)
		134.0	
$(19/2^+)$	836.2	333.7	3.7(4)
		199.8	
$(21/2^+)$	986.9	350.5	7.7(11)
		150.7	
$(23/2^+)$	1251.8	415.6	
		265	
$(25/2^+)$	1410.7	423.8	
		159	
$(27/2^+)$	1748	496	
		337	
$(29/2^+)$	1907	496	
		^{159}Gd	
$5/2^+$	67.8		
$7/2^+$	118.7		
$9/2^+$	185.3		
$11/2^+$	273.9	155.1	0.64(8)
		88.6	
$13/2^+$	372.4	187.1	0.63(9)
		98.4	
$(15/2^+)$	507.5	233.6	1.38(15)
		135.1	
$(17/2^+)$	633.4	261.0	2.4(4)
		125.7	
$(19/2^+)$	824.0	316.5	2.6(6)
		190.8	
$(21/2^+)$	969.4	336.0	
		145.1	
$(23/2^+)$	1224.3	400.3	
		255.1	
$(25/2^+)$	1379.5	410.1	
		155.2	
$(27/2^+)$	1705	481	
		326	
$(29/2^+)$	1863	483	
$(31/2^+)$	2263	558	
$(33/2^+)$	2414	551	

^{a}Spin and parity of the depopulated state.
^{b}Branching ratio, $\lambda = I_\gamma(I \to I-2)/I_\gamma(I \to I-1)$, where I_γ is the intensity of the transition.
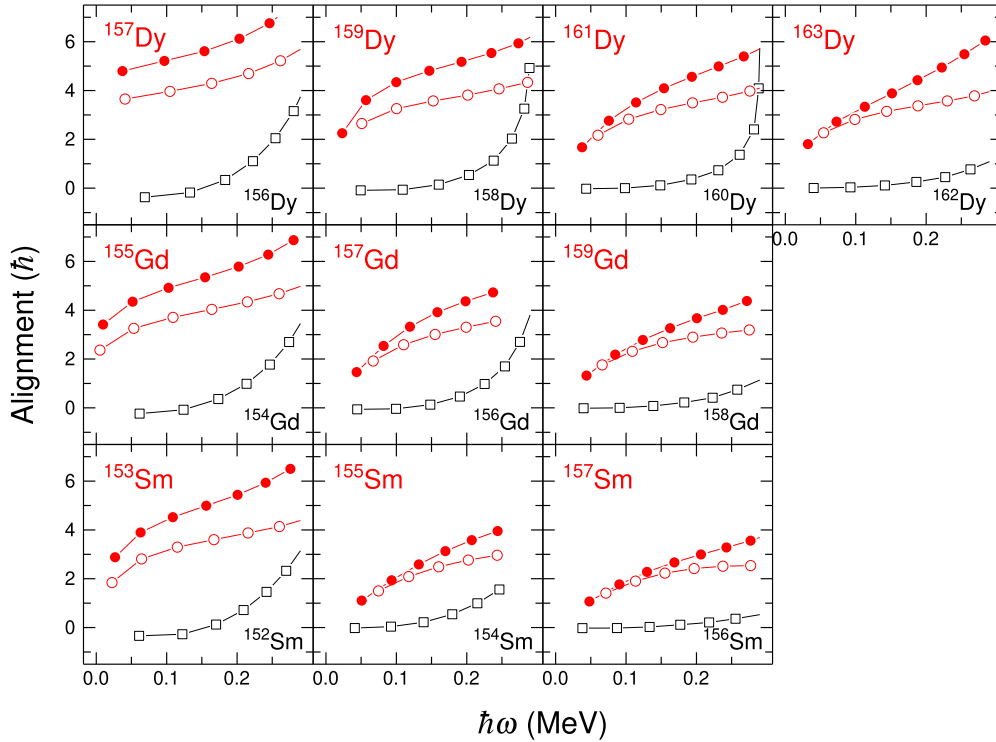
FIG. 4. Alignments for the $\nu i_{13/2}$ bands (red circles) in the $N = 91$, 93, 95, and 97 isotopes of Sm, Gd, and Dy. Different Harris parameters were used in each case in order to remove the angular momentum generated by the core, as is demonstrated by the nearly zero alignment values displayed at low frequency by the $N - 1$, even-even ground-state bands (black squares). The solid (empty) circles represent the $\alpha = +1/2$ ($\alpha = -1/2$) signature.

circles, and the $\alpha = -1/2$ ones as empty circles. In Fig. 4, the bands assigned to ^{155}Sm and ^{159}Gd exhibit an immediate gain in alignment, which mirrors the behavior seen in the nearby nuclei, herewith justifying further their $\nu i_{13/2}$ assignment.

In addition to aiding with the configuration assignment, the systematic plot of Fig. 4 presents a clear difference between ^{157}Dy and the other nuclei displayed in the figure. The initial alignment values (near $\hbar\omega = 0.05$ MeV) are slightly lower in ^{155}Gd and ^{153}Sm compared to ^{157}Dy; and they are significantly lower in the $N = 93$, 95, and 97 cases, with values ranging between 1–2 $\hbar$ relative to the ground-state bands of their $N - 1$, even-even neighbor. It should be noted that this effect is not dependent on the exact choice of Harris parameters. As these bands result from a $j = 13/2$ shell and have an angular momentum projection on the symmetry axis of $K = 5/2$, one would a priori expect to observe a much higher initial alignment value for these sequences. Indeed, their initial alignment values should be closer to that observed in ^{157}Dy of approximately 4–5 $\hbar$. This raises the question of what could systematically cause the initial alignment values to be lower than expected for all of these nuclei.

The possible answer may be found from transfer reaction studies of ^{153}Sm [20,21] and ^{155}Gd [22] performed approximately 50 years ago. These works determined that the yrast, positive-parity sequence is substantially mixed between the $i_{13/2}$ 3/2[651] and $d_{3/2}$ 3/2[402] configurations. A structure purely based on the 3/2[402] orbital would likely have nearly zero initial alignment, since j and K are equal. The mixing of the $i_{13/2}$ and $d_{3/2}$ orbitals would lead to a smaller than

expected initial alignment for the $i_{13/2}$ band, consistent with the observations in Fig. 4. It is possible that similar mixing occurs in all of the nuclei shown in the figure (except for ^{157}Dy) to explain the initially low alignment values. The distinctive increase in alignment in the low-frequency region likely indicates that the amount of mixing between the two configurations decreases as the nuclei rotate with higher frequency. Theoretical calculations investigating the amount of mixing, as well as the frequency dependency of the mixing, between the $i_{13/2}$ and $d_{3/2}$ orbitals would be enlightening to further justify this interpretation.

If mixing between the $i_{13/2}$ and $d_{3/2}$ configurations is indeed the reason for the surprisingly low initial alignment, it implies that the 3/2[402] orbital likely remains near the Fermi surfaces of the Sm, Gd, and Dy nuclei with $N = 91$, 93, 95, and 97. Figure 5 displays the single-neutron energies in the rare-earth region versus deformation β_2. The $i_{13/2}$ orbitals are strongly down sloping with deformation, while the 3/2[402] one is strongly up sloping as can be seen in the lower right-hand corner of Fig. 5. As N increases for a given isotope, its deformation increases (since the Fermi surface moves further away from the $N = 82$ spherical shell gap). Therefore, the Fermi surfaces move up to the right in Fig. 5, as shown for illustrative purposes by the red, horizontal bars. The 3/2[402] orbital may lie closer to the 11/2[505] one than it appears in Fig. 5, such that the neutron Fermi surface and the up-sloping 3/2[402] orbital may indeed track each other from $N = 91$ to $N = 97$ and this would account for the systematic trends observed in Fig. 4.
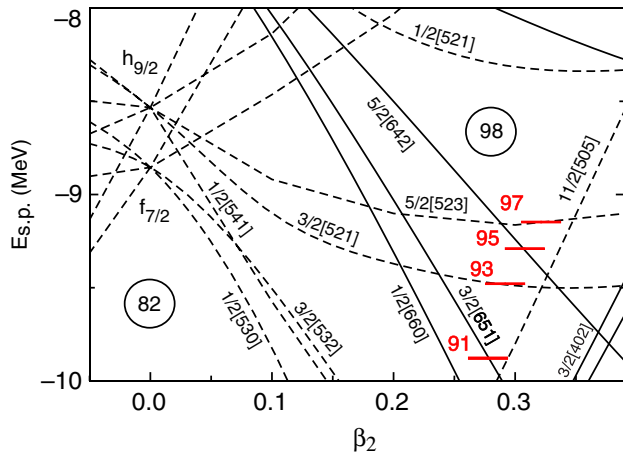
FIG. 5. Single-particle energies versus deformation (β_2) for neutrons in the rare-earth region using a Woods-Saxon potential. Possible locations of the $N = 91$, 93, 95, and 97 Fermi surfaces are indicated as red, horizontal bars in the figure. These are not exact locations; however, they illustrate the possible movement of the Fermi surfaces as N and β_2 increase.

Another characteristic feature of $\nu i_{13/2}$ bands can be observed in Fig. 6 as an energy difference between the $\alpha = +1/2$ ($I = 5/2, 9/2, 13/2$ $etc.$) and $\alpha = -1/2$ ($I = 7/2, 11/2, 15/2$ $etc.$) signatures. This energy separation is known as signature splitting, and can be is defined using the equation

$$S(I) = E(I) - (E - 1) - \tfrac{1}{2}[E(I + 1)$$
$$- E(I) + E(I - 1) - E(I - 2)], \quad (1)$$

where $E(I)$ is the energy of the state (in keV) at spin I. The signature splitting of the $\nu i_{13/2}$ bands in the $N = 93$ and 95 isotones of the even-Z nuclei in this region have been plotted in Figs. 6(a) and 6(b), respectively. The data from the following references were used for Fig. 6: ^{151}Ce$_{93}$ [11], ^{153}Nd$_{93}$ [11], ^{157}Gd$_{93}$ [16], ^{159}Dy$_{93}$ [18], ^{161}Er$_{93}$ [23], ^{163}Yb$_{93}$ [24], ^{155}Nd$_{95}$ [6], ^{157}Sm$_{95}$ [14], ^{161}Dy$_{95}$ [18], ^{163}Er$_{95}$ [25], and ^{165}Yb$_{95}$ [26]. In order to focus on the degree of splitting observed at low spin (before any band crossing), the values shown in Fig. 6 were limited to spins below 29/2. The $\alpha = +1/2$ signature is lower in energy and, therefore, has negative values in Fig. 6, while the $\alpha = -1/2$ one is unfavored and has positive values.

Signature splitting is a result of the presence of the decoupling constant, which only exists for a $K = 1/2$ orbital in any given shell [27]. However, Coriolis mixing occurs between the different orbitals of a shell such that higher K members can exhibit signature splitting as well. Therefore, even though the bands in Fig. 6 are likely based on the $K = 5/2$ orbital, they all have a $K = 1/2$ component in their wave function, which is the cause of the energy staggering between the signatures. In fact, the magnitude of the energy splitting is an indication of how prevalent the $K = 1/2$ component is mixed in a specific sequence. A large degree of splitting indicates a significant amount of $K = 1/2$ mixing, and implies that this orbital is near the Fermi surface. Indeed, one may notice that in Fig. 6, the magnitude of the splitting in the $N = 93$ nucleus of a given Z is larger than in its $N = 95$ isotope. This is due to the fact
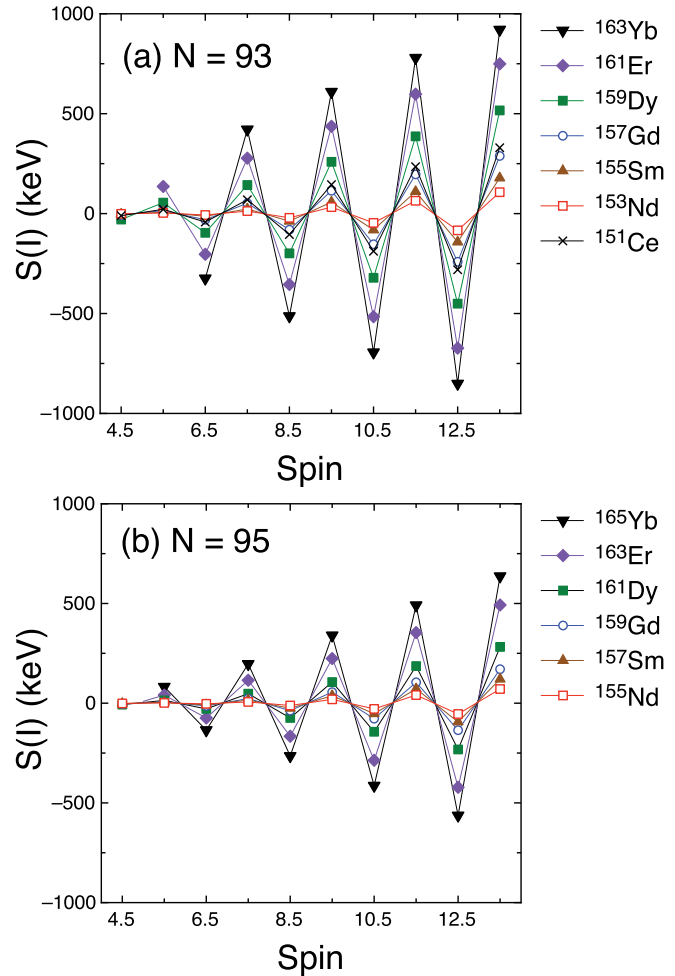

FIG. 6. Signature splitting (as defined in the text) versus spin for the $\nu i_{13/2}$ bands in even-Z, rare-earth nuclei that have (a) $N = 93$ and (b) $N = 95$.

that the $N = 93$ Fermi surface lies closer to the $\nu i_{13/2} 1/2[660]$ orbital in comparison to $N = 95$, as seen in the Woods-Saxon diagram of Fig. 5.

It should be noted that the mixing of the $3/2[402]$ orbital with the $i_{13/2}$ band will also affect the magnitude of the signature splitting. As previously stated, this mixing is likely most prevalent at low frequencies; therefore, the small splitting observed at the lowest spins in Fig. 6 is consistent with the influence of the $3/2[402]$ configuration. However, as stated above, the mixing of the $3/2[402]$ orbital likely decreases with spin and will play a smaller role in the observed splitting at the higher spin values shown in Fig. 6.

One can easily observe a trend in both the $N = 93$ and 95 isotones of Fig. 6, where the magnitude of the signature splitting reduces as Z decreases toward 60. This suggests a reduction with Z of the $K = 1/2$ component in the wave functions of these bands. The $K = 1/2$ orbital rapidly decreases in energy as deformation (β_2) increases (see Fig. 5). Therefore, the reduction in the size of the signature splitting as Z decreases can be associated with a persistent increase in deformation from ytterbium to neodymium ($Z = 60$) for both $N = 93$ and 95. It is interesting to note in Fig. 6(a) that

the magnitude of splitting increases for $Z = 58$, ^{151}Ce, which indicates that the minimum splitting is indeed observed in neodymium. That is, the maximum deformation in the $N = 93$ and 95 isotones is not at midshell ($Z = 66$), but rather at $Z = 60$, a finding consistent with the $E(2^+)$ values. Therefore, there is appreciable experimental evidence of a deformed, subshell gap at $Z = 60$, although more direct experimental indicators (e.g., observing large energy gaps between Nilsson proton states in nuclei near neodymium and/or systematic lifetime measurements in this region) are required to further substantiate this assertion.

V. SUMMARY

The ^{160}Gd + ^{154}Sm reaction produced excited states in ^{159}Gd and ^{155}Sm via one-neutron transfer. In both of these nuclei, the lone observed decay sequence that could be identified is based on an $i_{13/2}$ quasineutron. Signature splitting is a known characteristic of these $\nu i_{13/2}$ bands, and a systematic investigation of this feature in the $N = 93$ and 95 isotones

suggests that deformation increases from $Z = 70$ (Yb) to 60 (Nd). As a result, the maximum deformation is not at the proton midshell, but rather at $Z = 60$ as a consequence of a deformed subshell gap. Further experimental information is required to investigate this possibility.

[1] Z. Patel *et al.*, Phys. Rev. Lett. **113**, 262502 (2014).

[2] D. J. Hartley, F. G. Kondev, R. Orford, J. A. Clark, G. Savard, A. D. Ayangeakaa, S. Bottoni, F. Buchinger, M. T. Burkey, M. P. Carpenter, P. Copp, D. A. Gorelov, K. Hicks, C. R. Hoffman, C. Hu, R. V. F. Janssens, J. W. Klimes, T. Lauritsen, J. Sethi, D. Seweryniak *et al.*, Phys. Rev. Lett. **120**, 182502 (2018).

[3] L. Satpathy and S. K. Patra, Nucl. Phys. A **722**, C24 (2003).

[4] E. F. Jones, J. H. Hamilton, P. M. Gore, A. V. Ramayya, J. K. Hwang, A. P. de Lima, S. J. Zhu, Y. Z. Luo, C. J. Beyer, J. Kormicki, X. Q. Zhang, W. C. Ma, I. Y. Lee, J. O. Rasmussen, S. C. Wu, T. N. Ginter, P. Fallon, M. Stoyer, J. D. Cole, A. V. Daniel *et al.*, J. Phys. G: Nucl. Part. Phys. **30**, L43 (2004).

[5] R. Yokoyama, S. Go, D. Kameda, T. Kudo, N. Inabe, N. Fukuda *et al.*, Phys. Rev. C **95**, 034313 (2017).

[6] J. M. Eldridge, E. H. Wang, C. J. Zachary, J. H. Hamilton, B. M. Musangu, A. V. Ramayya, G. M. Ter-Akopian, Yu. Ts. Oganessian, Y. X. Luo, J. O. Rasmussen, and S. J. Zhu, Phys. Rev. C **102**, 044323 (2020).

[7] W. Urban, T. Rząca-Urban, A. G. Smith, G. S. Simpson, and J. P. Greene, Phys. Rev. C **102**, 064321 (2020).

[8] S. J. Asztalos, I. Y. Lee, K. Vetter, B. Cederwall, R. M. Clark, M. A. Deleplanque, R. M. Diamond, P. Fallon, K. Jing, L. Phair, A. O. Macchiavelli, J. O. Rasmussen, F. S. Stephens, G. J. Wozniak, J. A. Becker, L. A. Bernstein, D. P. McNabb, P. F. Hua, D. G. Sarantites, J. X. Saladin *et al.*, Phys. Rev. C **60**, 044307 (1999).

[9] R. V. F. Janssens and F. S. Stephens, Nucl. Phys. News **6**, 9 (1996).

[10] D. C. Radford, Nucl. Instrum. Methods Phys. Res. A **361**, 297 (1995).

[11] G. S. Simpson, W. Urban, J. A. Pinston, J. C. Angelique, I. Deloncle, H. R. Faust, J. Genevey, U. Köster, T. Materna, R. Orlandi, A. Scherillo, A. G. Smith, J. F. Smith, T. Rząca-Urban, I. Ahmad, and J. P. Greene, Phys. Rev. C **81**, 024313 (2010).

[12] N. Nica, Nucl. Data Sheets **160**, 1 (2019).

[13] C. W. Reich, Nucl. Data Sheets **113**, 157 (2012).

[14] C. J. Zachary, Ph.D. thesis, Vanderbilt University, 2019.

[15] T. Hayakawa, M. Oshima, Y. Hatsukawa, J. Katakura, H. Iimura, M. Matsuda, S. Mitarai, Y. R. Shimizu, S.-I. Ohtsubo,

T. Shizuma, M. Sugawara, and H. Kusakari, Nucl. Phys. A **657**, 3 (1999).

[16] T. Hayakawa, Y. Toh, M. Oshima, M. Matsuda, Y. Hatsukawa, N. Shinohara, H. Iimura, T. Shizuma, Y. H. Zhang, M. Sugawara, and H. Kusakari, Phys. Lett. B **551**, 79 (2003).

[17] A. Pipidis, M. A. Riley, J. Simpson, R. V. F. Janssens, F. G. Kondev, D. E. Appelbe, A. P. Bagshaw, M. A. Bentley, T. B. Brown, M. P. Carpenter, D. M. Cullen, D. B. Campbell, P. J. Dagnall, P. Fallon, S. M. Fischer, G. B. Hagemann, D. J. Hartley, K. Lagergren, R. W. Laird, T. Lauritsen *et al.*, Phys. Rev. C **72**, 064307 (2005).

[18] A. Jungclaus, B. Binder, A. Dietrich, T. Härtlein, H. Bauer, Ch. Gund, D. Pansegrau, D. Schwalm, D. Bazzacco, E. Farnea, S. Lunardi, C. Rossi-Alvarez, C. Ur, G. de Angelis, A. Gadea, D. R. Napoli, X. R. Zhou, and Y. Sun, Phys. Rev. C **67**, 034302 (2003).

[19] S. M. Harris, Phys. Rev. **138**, B509 (1965).

[20] M. J. Bennett, R. K. Sheline, and Y. Shida, Nucl. Phys. A **171**, 113 (1971).

[21] I. Kaneström and P. O. Tjöm, Nucl. Phys. A **179**, 305 (1972).

[22] M. E. Bunker and C. W. Reich, Phys. Lett. B **25**, 396 (1967).

[23] J. D. Garrett, G. B. Hagemann, B. Herskind, J. Bacelar, R. Chapman, J. C. Lisle, J. N. Mo, A. Simcock, J. C. Willmott, and H. G. Price, Phys. Lett. B **118**, 297 (1982).

[24] J. Kownacki, J. D. Garrett, J. J. Gaardhøje, G. B. Hagemann, B. Herskind, S. Jónsson, N. Roy, H. Ryde, and W. Waluś, Nucl. Phys. A **394**, 269 (1983).

[25] G. B. Hagemann, H. Ryde, P. Bosetti, A. Brockstedt, H. Carlsson, L. P. Ekström, A. Nordlund, R. A. Bark, B. Herskind, S. Leoni, A. Bracco, F. Camera, S. Frattini, M. Mattiuzzi, B. Million, C. Rossi-Alvarez, G. de Angelis, D. Bazzacco, S. Lunardi, and M. De Poli, Nucl. Phys. A **618**, 199 (1997).

[26] L. L. Riedinger, G. J. Smith, P. H. Stelson, E. Eichler, G. B. Hagemann, D. C. Hensley, N. R. Johnson, R. L. Robinson, and R. O. Stoyer, Phys. Rev. Lett. **33**, 1346 (1974).

[27] R. F. Casten, *Nuclear Structure from a Simple Perspective* (Oxford University Press, New York, 1990).